
The geometry of hidden representations of large transformer models

Lucrezia Valeriani^{1,2} Diego Doimo³ Francesca Cuturello¹ Alessandro Laio^{3,4}
Alessio Ansuini^{1,*} Alberto Cazzaniga^{1,*}

¹ AREA Science Park, Padriciano 99, 34149 Trieste, Italy

² University of Trieste, Trieste 34127, Italy

³ SISSA, via Bonomea 265, 34136 Trieste, Italy

⁴ ICTP, Strada Costiera 11, 34014 Trieste, Italy

* **Correspondence:**

alessio.ansuini@areasciencepark.it

alberto.cazzaniga@areasciencepark.it

Abstract

Large transformers are powerful architectures for self-supervised analysis of data of various nature, ranging from protein sequences to text to images. In these models, the data representation in the hidden layers live in the same space, and the semantic structure of the dataset emerges by a sequence of functionally identical transformations between one representation and the next. We here characterize the geometric and statistical properties of these representations, focusing on the “evolution” of such properties across the layers. By analyzing geometric properties such as the intrinsic dimension (ID) and the neighbor composition we find that the representations evolve in a strikingly similar manner in transformers trained on protein language tasks and image reconstruction tasks. In the first layers, the data manifold “expands”, becoming high-dimensional, and then it contracts significantly in the intermediate layers. In the last part of the model, the ID remains approximately constant or forms a second shallow peak. We show that the semantic complexity of the dataset emerges at the end of the first peak. This phenomenon can be observed across many models trained on diverse datasets. Based on these observations, we suggest using the ID profile as an unsupervised proxy to identify the layers which are more suitable for downstream learning tasks.

1 Introduction

In recent years, deep learning drastically changed the landscape of scientific research and technology, giving a new impulse to technical and scientific advancements in many disciplines.

A particular class of deep learning models, self-supervised models based on transformers, combine high predictive performance and architectural simplicity. These architectures have been heavily inspired by transformer-like models that emerged in natural language processing: they consist of a stack of identical self-attention blocks trained in a self-supervised fashion by minimizing a masked language model (MLM) objective [38, 13]. It has been shown that the features learned by these models, after suitable fine-tuning, can be used to solve a wide range of downstream tasks in natural language processing [27, 30, 6], biology [32, 15, 22, 20], and computer vision [8, 23, 29].

Analysis of other types of architectures highlighted that data representations in deep learning models undergo profound changes across the layers [3, 14]. In transformer models, each module maps the

data into a representation, and it has already been observed that the organization of representations in the last hidden layer can reflect abstract, domain-specific properties[8]. However, in models trained by self-supervision, the last representation has, by construction, the role to allow reconstruction of the input representation. Therefore, the most semantically rich representation will likely be deeper in the network.

In this paper, we systematically investigate, in some self-supervised models, fundamental geometric properties of representations, such as their intrinsic dimension (ID) and neighbor composition, and find robust within-domain behaviors, identifying similarities and differences across domains.

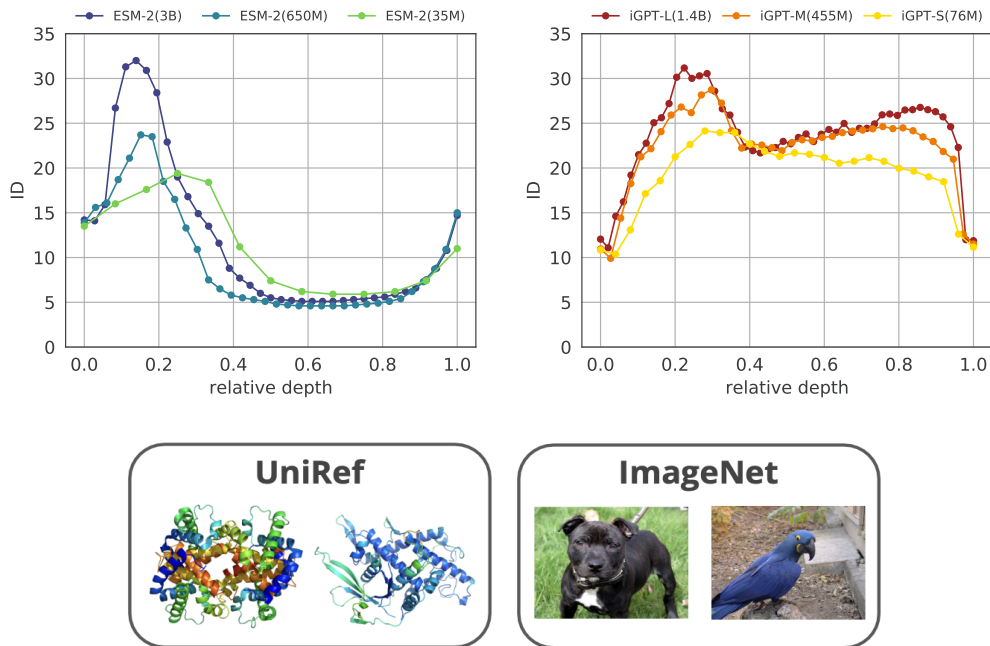


Figure 1: The intrinsic dimension (ID) of representations in hidden layers of large transformers, plotted against block number normalized by the total number of blocks (relative depth). [Left] The ID profile of ESM-2 protein language models of small (35M, green), medium (650M, blue), and large (3B, purple) sizes show a peak in the first part of the network, a long plateau, and a final ascent. [Right] The ID profile in iGPT models of small (76M, yellow), medium (455M, orange), and large (1.4B, red) sizes also an early followed by a less pronounced second peak for the medium and large model.

Our main results are:

- representations in large transformers evolve across the layers in distinct phases, revealed by simultaneous changes in global ID (section 3.1) and local neighborhood composition (section 3.2);
- a common trait of the ID profiles is a prominent peak of the ID, in which the neighbor structure is profoundly rearranged, followed by relatively low ID regions in which the representations encode abstract semantic information, such as the class label for images (section 3.2.2), remote homology for proteins (section 3.2.1); this abstract information emerge gradually while the ID decreases (section 3.1.4);
- the ID profile can be used to identify in an unsupervised manner the layers encoding the optimal representation for downstream learning tasks, such as homology searches (section 3.2.1).

These findings suggest a general computational strategy learned by these models, in which the reconstruction task is performed in three phases: 1) a data expansion in a high intrinsic dimension space. This expansion resembles the strategy followed in kernel methods [34], where one implicitly

expands the feature space by introducing non-linear functions of the input features; 2) a compression phase that projects the data in low-dimensional, semantically meaningful representations. Strikingly, this representation emerges spontaneously in all the self-supervision tasks we considered; a decoding phase in which the minute decision-making needed to reconstruct the data from a compressed representation is performed. The layers performing this task behave similarly to the decoder layers in a “vanilla” autoencoder.

2 Methods

2.1 Intrinsic dimension

The *manifold hypothesis* is based on the observation that many datasets embedded in high dimensions, resulting from the observations of natural phenomena (images, sounds, etc.), lie close to low-dimensional manifolds. The intrinsic dimension of a dataset is the dimensionality of the embedded manifold approximating the data; in other words, the ID is the minimum number of coordinates that allow specifying a data point approximately without information loss. We adopt the global estimator “TwoNN” of the ID developed in [16], which requires only local information on the distance to the first (r_1) and second (r_2) nearest neighbors of each data point, and that works under the mild assumption of approximately locally constant density. In such a case, the theoretical cumulative distribution F of the ratio $\mu = r_2/r_1$ can be explicitly derived from the ground truth ID without information on the density; after approximating F with the empirical cumulate calculated on the dataset, one can estimate the intrinsic dimension. We refer to A.2 for a description of the implementation adopted in our analyses. The TwoNN algorithm is robust to changes in curvature and density, and it is asymptotically correct in the range in which the ground truth ID is < 30 . The TwoNN estimator has already been employed to analyze representations in deep convolutional networks in [3]. In the range of IDs that we observe, the TwoNN algorithm slightly underestimates larger values [19], without any consequence on the description of the phenomena we observe.

2.2 Neighborhood overlap

The local changes in data representation across the model can be traced in the rearrangement of the neighbor structure of the data space under the transformation induced by each block: points that are close in one layer may not be so in the following layer, and *viceversa*. The neighborhood overlap [14] measures the degree of similarity of two data representations by computing the common fraction of points that are k -nearest neighbors in both representations. Explicitly, given a dataset with N elements, consider the k points nearest to an element x^i of the dataset at a given layer l , and let A^l be the adjacency matrix with entries $A^l_{ij} = 1$ if x^j is a neighbor of x^i and 0 otherwise. The neighbor overlap between layers l and m is defined as $\chi_k^{l,m} = \frac{1}{N} \sum_i \frac{1}{k} \sum_j A^l_{ij} A^m_{ij}$, and it is easily seen to lie in $[0, 1]$. The neighborhood overlap can be generalized in the following way. Let us consider a function f that associates a characteristic of interest to each data point. We can use f to define a neighborhood through the adjacency matrix $A^f_{ij} = 1$ if $f(x^i) = f(x^j)$ and 0 otherwise. In this case, $\chi_k^{l,f} = \frac{1}{N} \sum_i \frac{1}{k} \sum_j A^l_{ij} A^f_{ij}$ is the average fraction of neighbors of a given point in layer l that have the same property f as the central point. A particularly interesting case arise when f is a ground truth classification label. For protein language models we focus on ground truth classes of biological interest such as the protein super-family of the SCOPe dataset in 3.2.1, where we analyze the local structure considering $k = 10$ neighbors. In section 3.2.1, we also discuss the case $k = 1$, where the measure collapses to the accuracy of first hit retrieval recently considered in [35]. For image transformer models we focus on classes defining the semantic classification of the Imagenet dataset and we analyze the neighborhood composition within the first $k = 30$ nearest neighbor in section 3.2.2.

2.3 Models and Datasets

2.3.1 Transformer models for protein sequences

The single-sequence protein language models (pLMs) we analyze are essentially characterized by the same architecture: after a learned positional encoding of the data, a stack of identical self-attention blocks transforms the input creating a sequence of representations. These models are trained in a

self-supervised way to perform a partial input reconstruction task by minimizing masked language model loss. As a byproduct, the learned representations are rich in biological information. More in detail, the input data points, corresponding to proteins, are variable-length sequences of l letters $s = a_1, a_2, \dots, a_l$, chosen from an alphabet of $n_a (\simeq 20)$ tokens corresponding to amino acids. Each token is encoded by an embedding layer into a vector of size d so that the generic protein s is represented as a matrix $x := f_0(x)$ of size $l \times d$. A model with B blocks transforms a data point $x \in \mathbb{R}^{l \times d}$ into a sequence of representations: $f_0(x) \rightarrow f_1(x) \rightarrow \dots \rightarrow f_B(x) \rightarrow f_{out}(x)$, where $f_i, i = 1, \dots, B$ stands for the self-attention module at the i -th block, and the final LM-head f_{out} is a learned projection onto dimension $l \times n_a$. The size of each hidden layer does not change across the model and is equal to $l \times d$; therefore, the action of the model is a sequence of mappings $\mathbb{R}^{l \times d} \rightarrow \mathbb{R}^{l \times d}$. The representation of a protein across the network consists of a collection of l vectors that change across the layers, and several strategies for comparing variable length sequences have been investigated [12]. For each layer i we choose to perform global average pooling across the row dimension $f_i(x) \rightarrow \frac{1}{l} \sum_{j=1}^l (f_i(x))_j$, since this reduction retrieves sufficient biological information to solve, directly or possibly after fine-tuning, homology, structural and evolutionary tasks. For a given pLM, the action of the network on a dataset of N proteins can thus be described by $B + 1$ collections of N vectors in \mathbb{R}^d : these are the data representations that we investigate. In our applications, we focus on representations obtained starting from the datasets ProteinNet and SCOPe described in detail in section 2.3.3. We consider a selection of models from the ESM-2 family pre-trained on UniRef50 [10], whose properties are detailed in Table 1 in the Appendix.

2.3.2 Transformer models for image processing

The structure of the Image GPT (iGPT) transformers is very similar to that of pLMs. We analyze architectures pre-trained on ImageNet with an autoregressive loss to generate images. Due to the high memory footprint required by the attention layers, the image resolution is reduced and the three color channels are encoded in an “embedding axis” with size $d_{in} = 512$. In practice, the \mathbb{R}^3 color space in which each pixel is represented by a triplet of real numbers (R, G, B) is quantized with k -means clustering ($k = 512$), and each pixel is described by the *discrete* “code” of the cluster where it belongs. An input image is then represented by a data point $x \in \mathbb{R}^{l \times d_{in}}$ where the l pixels are placed along the sequence axis in raster order and d_{in} encodes the color of each pixel. Like in pLMs, an input data point, after the embedding layers, is processed by a stack of attention blocks that produce a sequence of data representations of identical size $x \in \mathbb{R}^{l \times d}$. The final head f_{out} projects the output of the last attention block to $\mathbb{R}^{l \times d_{in}}$, which encodes at each sequence position i the conditional distribution

$$p(x_i) = p(x_i | x_0, \dots, x_{i-1}) \quad (1)$$

Once the network is trained, an image can be generated by sampling from $p(x_i)$ one pixel at a time. As in pLMs we extract the hidden image representations by averaging over the sequence dimension. More precisely we extract the representations after the first normalization layer of the attention blocks. This reduced representation is also used in [8] to measure the representation quality with linear probes.

2.3.3 Datasets

For the analysis of pLMs, we consider two benchmark datasets: ProteinNet and SCOPe. ProteinNet [2] is a standardized dataset for evaluating protein sequence-structure relationships. The ProteinNet training set, composed of 25299 sequences, will be our reference for extracting the pLM representations for the analysis of the characteristic ID curves in Fig. 1, and for the computation of neighborhood overlap of consecutive layers in Fig. 2. The Astral SCOPe v2.08 (SCOPe) dataset [7] contains genetic domain sequence subsets filtered to obtain $< 40\%$ pairwise sequence identity. Each domain is hierarchically classified into fold, super-family, and family. Following the filtering procedure recommended in [36], we obtain a dataset composed of 14535 sequences. For defining the remote homology task, which consists of a class subdivision of proteins by structural similarity induced by common ancestry, we select proteins in the SCOPe dataset belonging to super-families with at least ten elements, and we ensure that each super-family is composed of at least two families. We thus obtain a dataset composed of 10256 sequences grouped in 288 super-families. At evaluation time, when computing the k -NN of a given protein domain we remove elements in the same family to ensure we are considering only sufficiently remote homologs.

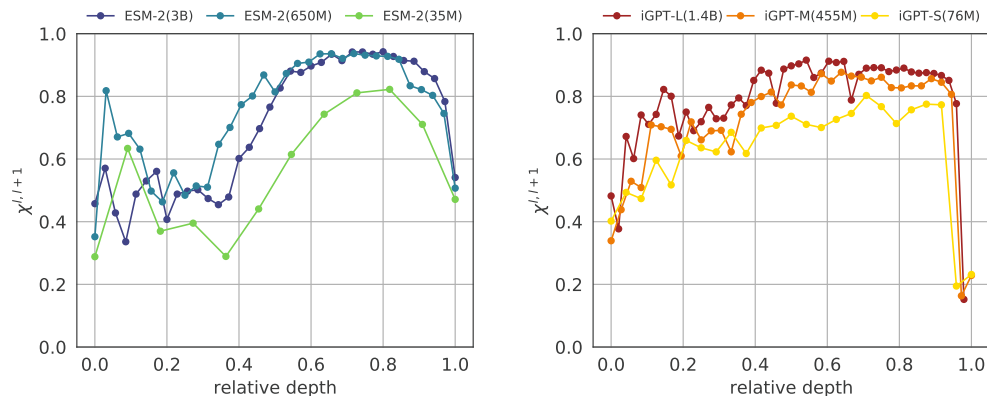


Figure 2: The neighborhood rearrangement across the layers in large transformers. [Left] Neighborhood overlap of consecutive layers $\chi^{l,l+1}$, computed for ESM-2(35M, green), ESM-2(650M, blue), and ESM-2(3B, purple), shows major local rearrangements in the layers corresponding to the peak and in the final layers and minor changes in the plateau region, mirroring the behaviour of the ID. [Right] The trend of $\chi^{l,l+1}$ in iGPT-S (yellow), iGPT-M (orange), and iGPT-L (red) is similar to pLMs: the neighborhood composition changes more in early layers where the ID reaches a peak and in the final layers.

For the analysis of the iGPT representations, we choose 90000 images from the ImageNet training set [11]. We select at random 300 classes and keep 300 images per class.

3 Results

3.1 The intrinsic dimension profile in large transformers is similar in different tasks and architectures

In large transformers, the input representation is processed in a sequence of identical blocks, creating a sequence of representations living in the same space but radically different in their geometrical properties and semantic content. We start by estimating the ID of each representation for large transformers trained by self-supervision on protein language and image reconstruction tasks. The ID profiles provide a glimpse into the geometry of the manifolds in which the data are embedded. As we will see the ID changes through the layers in a highly non-trivial manner, with three phases that can be recognized in all the transformers and a fourth phase which we observed only in the iGPT models. In the following sections, we will see how these phases signal the development of structured semantic content in intermediate representations, which are hidden instead in the input and, by construction, in the final embeddings.

3.1.1 Protein language models

After each self-attention block, we extract representations for proteins in the ProteinNet dataset 2.3.3, and plot their ID against the block number, normalizing with respect to the total number of blocks, referred to as *relative depth*. In Fig. 1 [Left], we report the results for pLMs in the ESM-2 model family with 35M, 650M, and 3B parameters. These models have been publicly released at <https://github.com/facebookresearch/esm>. Analogous results for models trained on different datasets are reported in the Appendix A.3.1.

The typical shape of the ID curve has three distinct phases: a peak phase, a plateau phase, and a final ascent phase. The peak develops in early layers and occupies approximately the first third of the curve. In this phase, the ID rapidly expands, and after reaching a maximum in an ID range of a few tenths, it rapidly contracts. After achieving its maximum, the ID is compressed to remarkably low values that characterize the plateau, where the ID remains approximately stationary, reaching values of $\sim 6 - 7$ at the elbow before the final ascent. In the final ascent, the ID grows again, going back progressively to values close to the ID computed on the input representation after the positional

embedding. The ID undergoes major changes across hidden layers: a ratio of $\sim 4 - 5$ of the ID values can be observed between the minima at the plateau and maxima at the peak. These changes are even more remarkable since the embedding dimension d remains unchanged across all the layers, depending only on the architecture (see column “Emb. Dim.” of Table 1 in the Appendix).

This behavior is preserved when changing the scale of the model, assuming that one considers sufficiently expressive architectures of size $\gtrsim 35\text{M}$. The maximum reached by the ID during the peak phase tends to increase moderately with the size of the models. In the plateau phase, we find a remarkable quantitative consensus on ID values which are approximately identical in models spanning two orders of magnitude in size, with number of parameters ranging from 35M to 3B, and with different values of extrinsic dimensionality d , ranging between 480 and 2560. Models with a sufficiently large number of parameters ($> 35\text{M}$), or equivalently expressive enough models, essentially recover the initial ID after the last self-attention block. This is tightly related to the self-supervised task focused on the local recovery of the missing tokens using the information from the context.

3.1.2 Image transformers

Fig. 1 [Right] shows the ID profiles of iGPT models of increasing size. We analyze the small (S), medium (M), and large (L) versions of iGPT trained on ImageNet. These models have been publicly released at (<https://github.com/openai/image-gpt>) and have 76M, 455M and 1.4B parameters respectively.

In all cases, the IDs of the output are similar to those of the input, consistently with what is observed in the protein language models. In the smallest iGPT network, the ID profile has a hunchback shape quite similar to that in convolutional models [3] trained on image classification. It is interesting to notice that the value of the ID at the peak is ~ 30 , much smaller than the value observed in convolutional architecture trained on the same dataset. Apparently, transformer-like architectures are able to find a more compact encoding of the input. This might be partially due to the difference in the embedding dimension, which in the iGPT transformer is constant with values in the range 512-1536 while in convolutional architectures it changes between layers and is much larger, ranging between $O(10^4)$ and $O(10^6)$. In the iGPT-M and iGPT-L model, the ID profile in the first part of the network is very similar to the profile observed in protein language models: the ID first grows significantly, reaching a maximum of ~ 32 after the first 25% of the layers. Afterward, the ID decreases, reaching a minimum of 25 after 40% of the layers. In the last part of the network, at variance with what is observed in pLMs, the ID does not remain constant but grows again (more moderately) forming a second shallow peak almost at the end of the network. Both peaks are more pronounced in the large architecture.

The results shown in Fig. 1 hint at a scenario that will be validated in the following: the ID is a proxy to semantic complexity. Therefore, the representation which should resemble more closely those extracted by supervised learning on the same datasets should be those corresponding to the relative minimum of the ID curve which follows the first peak. This minimum is well defined in iGPTs, while in pLMs the ID curve forms a plateau. We will see how this qualitative difference is reflected in the usefulness of the representation to perform *predictions*.

3.1.3 The neighborhood rearrangement across the layers mirrors the ID profile

We focus now on the study of the evolution of the data distribution across the layers. We characterize this evolution by monitoring the composition of the neighborhood of each data point across the layers. In particular, we monitor the neighborhood overlap $\chi_k^{l,l+1}$, defined in section 2.2, which measures the rate at which the neighborhood changes. In deep convolutional models, this rate is large only in the very last layers[14], where the representation is forced to become compliant with the ground-truth classification of the images.

In pLMs, we compute the neighborhood overlap on the representations of ProteinNet considered in Fig. 1 [Left]. Our analysis, whose results are reported in Fig. 2 [Left], shows that neighbor composition changes coherently with the behavior of the ID observed in section 3.1.1. This circumstance underlies an ID – neighborhood overlap relation that differs from what is found in convolutional architectures [14]. Quite remarkably, χ remains of order 0.5 in the first 40 % of the layers. This means that in each layer the neighborhood composition changes by $\sim 50 \%$, indicating that the representations

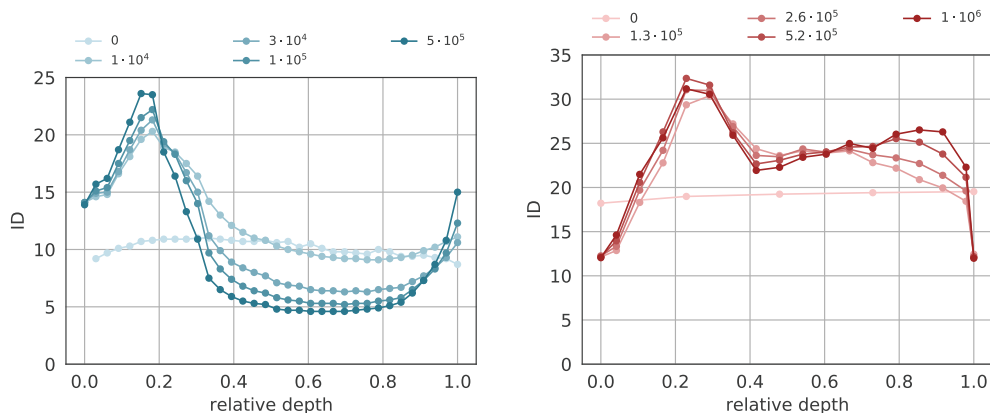


Figure 3: Evolution of ID curves during training. [Left] ID curves for the pLM ESM-2(650M) at checkpoints corresponding to $[0, 10^4, 3 \cdot 10^4, 10^5, 5 \cdot 10^5]$ training steps. Firstly, the peak develops; then the plateau reaches low-ID values and the ID in the final layers reaches values similar to the input. [Right] ID curves for iGPT-M (455M) at checkpoints $[0., 0.13, 0.26, 0.52, 1.] \cdot 10^6$ training steps. Firstly, the ID peak followed by a plateau with a local low-ID minimum develops; later in training a second peak emerges in the final layers.

are largely modified in every layer, in the first part of the network. This phase corresponds to the peak phase highlighted by the ID. In the plateau phase, the representations evolve at a much lower rate. In particular, for large enough models, the neighborhood composition changes very slowly, with more than 90% of neighbors shared across consecutive layers. The smallest model, characterized by low expressivity and high perplexity, constitutes an exception: the neighborhood composition in the plateau phase is, on average, less consistent, with major rearrangements also occurring in successive layers.

We perform a similar analysis for image transformers. In Fig. 2 [Right], we plot the neighborhood overlap as a function of the layer’s relative depth for iGPT models of different sizes. The profiles are qualitatively similar to those observed in protein language models, indicating a fast change in neighborhood composition in the first part of the network, where the first peak in the ID is observed. However, in iGPT transformers, the rate χ at which the neighborhood changes in the first part of the network is slightly smaller, bringing to values of χ of approximately 0.7. Also in iGPTs in the second part of the network neighborhood composition changes more slowly, with $\chi \simeq 0.9$. Similarly to pLMs, this behavior is more pronounced for models of high capacity, i.e., medium and large image transformers, since shallower models need faster rearrangements to achieve consistent results in fewer blocks. A large neighborhood rearrangement is always observed in the last layers, where the reconstruction task is carried on.

3.1.4 The evolution of the representations during training

Up to this point we focused on the evolution of geometric quantities across layers of fully trained models. We now shift our attention to the evolution of these quantities during training. In particular, we investigate how transformations of representations of the data manifold change during training for the pLM ESM-2(650M) and the image transformer iGPT-L model, reporting the results of our analysis in Fig. 3. We consider model-specific checkpoints during training depending on their availability.

In the case of the model ESM-2(650M), see Fig. 3 [Left], we analyze checkpoints corresponding to $[0, 1 \cdot 10^4, 3 \cdot 10^4, 1 \cdot 10^5, 5 \cdot 10^5]$ training iterations, where the last checkpoint is the converged model. At the beginning of training, the peak rapidly forms in lower layers, while the ID curve resembles the one of the untrained models in the remaining part of the network. Between $1 \cdot 10^4$ and $3 \cdot 10^4$ training steps, the ID of the plateau layers substantially decreases. In contrast, the ID measured in the last layers progressively increases towards the input ID. From $3 \cdot 10^4$ training steps to convergence, the ID curve reaches its final shape, with a slight increase of the ID measured at the peak and a further

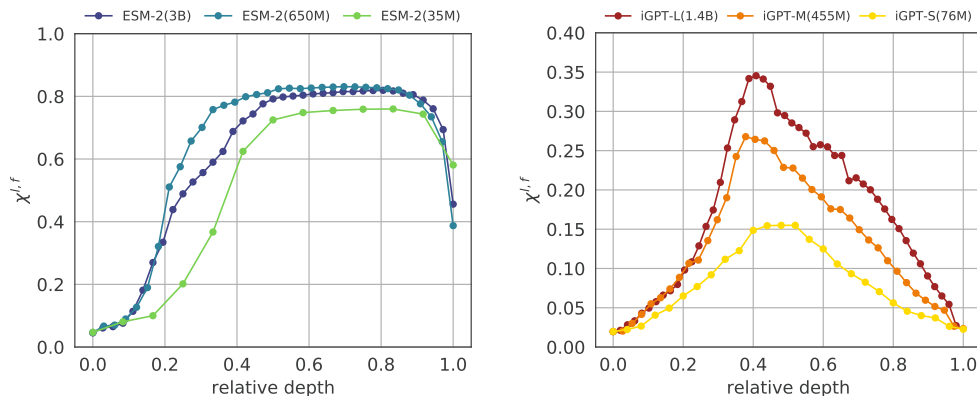


Figure 4: Local geometry and semantic relations in hidden representations. [Left] Overlap with remote homologs $\chi^{l,f}$ for ESM-2(35M, green), ESM-2(650M, blue), and ESM-2(3B, purple). Remote homology information is maximal in the plateau layers in correspondence with low ID values. [Right] Overlap with ground truth $\chi^{l,f}$ ImageNet labels for iGPT-S (yellow), iGPT-M (orange), and iGPT-L (red). The categorical information has a marked peak located in correspondence with the ID minimum.

slight compression at the plateau. The final ID curve is essentially acquired in two stages: at first, the initial ID peak emerges, and only later during training the data representation in the plateau layers is compressed to a low dimension; the latter behavior is tightly related to the emergence of semantic information that we discuss in 3.2.1.

In the case of iGPT-L, see Fig. 3 [Right], we consider instead the representations at checkpoints corresponding to $[0, 1.3 \cdot 10^5, 2.6 \cdot 10^5, 5.2 \cdot 10^5, 1 \cdot 10^6]$ training iterations. Before training the ID curve is flat, while at $1.3 \cdot 10^5$ training iterations the initial peak followed by a plateau precedes the return of the ID to the values at the input. In the remaining part of the training steps, while the dimension slightly increases at the initial peak and slightly decreases at the plateau, a second peak emerges in the last third of the hidden layers of the model.

3.2 The intermediate representations of large transformers are the most semantically rich

The most striking feature of the ID profiles shown in Fig. 1 is the presence of a sharp peak in the first part of the network, observed in all the models we considered. This peak in pLMs is followed by a long plateau covering more than half of the layers, and by a second shallow peak of the ID in the iGPT model (only in the smallest iGPT the second peak is absent). In transformers trained on image reconstruction tasks the ID at the minimum between the two peaks is similar to the one measured at the output of convolutional networks trained by supervised learning on the same data set[3]. This points to a scenario in which representations in the minimum encode semantic information on the datasets. The fact that features extracted in the intermediate layers of iGPT encode this information has been already demonstrated by other methods in ref [8]. We here extend this analysis to the protein language model, showing that in that case, the whole plateau is the region of the network where semantic information is maximum. Moreover, we show that the ID profile can be used to *predict* the layers where this information is maximally present.

3.2.1 The representation in the plateau region code remote homology relationships

Two proteins are said to be remote homologous if they correspond to highly dissimilar amino acid sequences while presenting a similar structure induced by common ancestry. It has been observed in [32] that Euclidean distances among representations in the last hidden layer of pLMs encode remote homology information. In Fig. 4 [Left] we study how this biological feature emerges in pLMs: considering representations of the SCOPE dataset, for every layer l we compute the neighborhood overlap $\chi_k^{l,f}$ where f is the classification by super-family, excluding neighbors in the same family to focus on remote homology. Structural homology information is absent in the positional embedding

layer; it grows smoothly in the peak phase reaching a stationary maximum $\chi_k^{l,f} \approx 0.8$ in the plateau phase, and it suddenly decreases in the final ascent phase. This analysis shows that homology information is maximal in the plateau layers, and it appears very early in the networks, in particular immediately after the peak of the ID. Remarkably, the predictivity of remote homology is significantly lower in the last hidden layer (0.4 against 0.8). The presence of these homology relationships can be exploited to perform predictions, and in particular to identify protein relationships: nearest neighbor searches for closest homologs in the plateau outperform SOTA methods based on last hidden layer representations by approximately 6% (see Appendix A.3.2 for further details).

3.2.2 Image semantic features emerge in the layer where the ID is minimum

It has been shown that predicting pixels in a self-supervised setting can generate representations that robustly encode semantic concepts, as it can be shown by linear probing and fine-tuning [8]. We complement these findings by showing that this remarkable property is connected with geometric aspects of representations: we quantify the semantic content of a representation by computing the overlap with the ground truth labels [14]. Similarly to the case of remote homology in pLMs, we find that the representations of iGPT models pre-trained on ImageNet that are richer in semantic information, having high overlap with the ground truth labels, are also the ones that correspond to a low ID. In Fig. 4 [Right] we plot the overlap of the representations, computed from the ImageNet training set, with their ground truth labels ($\chi^{l,f}$, $k = 30$); the results for the models iGPT-S (yellow), iGPT-M (orange), and iGPT-L (red) are shown. In all these cases, we consistently observe a peak of the overlap with the ground truth labels around a relative depth of ≈ 0.4 . However, this peak becomes sharper, and the overlap values higher, by increasing the size of the models (the peak value of $\chi^{l,f}$ is 0.15 in iGPT-S, 0.27 in iGPT-M, and 0.35 in iGPT-L). This is consistent with the location of the ID minima in the larger models iGPT-M and iGPT-L of Fig. 1 [Right], and, qualitatively, with the results in [8]. As we observed in pLM models, also in this case, the representations where the semantic abstractions are better encoded are also those where the ID is low.

4 Discussion and conclusions

In this work we investigate fundamental geometric properties of representations, such as the intrinsic dimension and the evolution across the layers of the neighbor structure, in large transformers models. The goal of this analysis is twofold: 1) understanding the computational strategies developed by these models to solve the self-supervised reconstruction task and 2) monitoring how high-level, abstract, information, such as remote homology in proteins and class labels in images, are related to geometrical properties of the representations.

The qualitative picture that emerges from our results is that large transformers behave essentially like sophisticated autoencoders, in which the data are first encoded into a low-dimensional and abstract representation, and are successively decoded from it. In the largest vision transformer, this similarity is particularly evident: a second peak in the ID profile is present, approximately mirroring the first, and the overlap with the ground truth labels also varies in an approximately symmetric manner in the first and in the second half of the network (Fig. 4 [Right]). This makes this model akin to a *symmetric* autoencoder, in which the decoder performs operations on the representations which are the inverse of those performed by the encoder. This scenario is only hinted by our analysis and should be validated by further experiments.

Crucially, the compression is preceded by an intrinsic dimensionality expansion and across the whole encoding process, the neighbors are rearranged at a relatively fast pace. The encoding, characterized by a peak in the ID and fast neighbors rearrangements is very similar across all the models we studied. The relation between a low intrinsic dimension at the end of the encoding part, and the richness in abstract content of representations is robust and quantitative in all the models we considered. It is also common to all the models a vast rearrangement of the neighbors in the layers close to the output. This occurs to deal with the *minutiae* of the decoding task and brings to a degradation of the abstract content.

The idea that hidden representations in the middle layers of large transformers models encode abstract information that can be leveraged to solve successfully a variety of tasks already appeared in the literature. In the field of natural language processing it has been observed that syntactic information is more prominent in the middle layers of deep transformers by syntactic tree depth reconstruction in

[18], and by the study of several NLP probes in [4, 5, 25, 37], reviewed also in [33]. As we already discussed in section 3, in [8] analogous considerations emerged in the context of large transformer models trained by autoregressive task on Imagenet. More recently these findings have been connected to the study of the geometry of representations in hidden layers. In particular, consistently with our findings, [1] show that pre-training implicitly minimizes the intrinsic dimension and that compression of information increases with the size of the model. [26], applying techniques from statistical mechanics developed in [9], relate the emergence of linear separability of manifolds in transformers for NLP to a combination of geometrical quantities, including dimensionality.

The analysis we performed can be further reinforced, for example, by analyzing the similarity of representations in the ID minima with those generated in supervised convolutional networks. This could allow gaining further understanding of the precise role of the second peak in the large iGPT model, and on the reason why it appears only in the latest phases of the training, and further insight for an explicit interpretation of low-ID representations in the plateau phase of pLMs.

Acknowledgements

The authors acknowledge AREA Science Park supercomputing platform ORFEO made available for conducting the research reported in this paper, and the technical support of the staff of the Laboratory of Data Engineering. We thank Roshan Rao and the Meta FAIR Protein Team for kindly providing the weights of the ESB-2(650M) models at training checkpoints used to produce Fig. 3 [Left].

L.V. was supported by the grant BOL “BIO Open Lab”. F.C. was supported by the grant PNRR “PRP@CERIC”. A.A. and A.C. were supported by the ARGO funding program.

References

- [1] Armen Aghajanyan, Sonal Gupta, and Luke Zettlemoyer. Intrinsic dimensionality explains the effectiveness of language model fine-tuning. In *Proceedings of the 59th Annual Meeting of the Association for Computational Linguistics and the 11th International Joint Conference on Natural Language Processing (Volume 1: Long Papers)*, pages 7319–7328, Online, August 2021. Association for Computational Linguistics.
- [2] Mohammed AlQuraishi. ProteinNet: a standardized data set for machine learning of protein structure. *BMC Bioinformatics*, 20, 2019.
- [3] Alessio Ansuini, Alessandro Laio, Jakob H Macke, and Davide Zoccolan. Intrinsic dimension of data representations in deep neural networks. *Advances in Neural Information Processing Systems*, 32, 2019.
- [4] Yonatan Belinkov, Lluís Marquez, Hassan Sajjad, Nadir Durrani, Fahim Dalvi, and James Glass. Evaluating layers of representation in neural machine translation on part-of-speech and semantic tagging tasks. In *Proceedings of the Eighth International Joint Conference on Natural Language Processing (Volume 1: Long Papers)*, pages 1–10, Taipei, Taiwan, November 2017. Asian Federation of Natural Language Processing.
- [5] T. Blevins, O. Levy, and L. Zettlemoyer. Deep rnns encode soft hierarchical syntax. *Proceedings of the 56th Association for Computational Linguistics (ACL)*, 2018.
- [6] Tom Brown, Benjamin Mann, Nick Ryder, Melanie Subbiah, Jared D Kaplan, Prafulla Dhariwal, Arvind Neelakantan, Pranav Shyam, Girish Sastry, Amanda Askell, Sandhini Agarwal, Ariel Herbert-Voss, Gretchen Krueger, Tom Henighan, Rewon Child, Aditya Ramesh, Daniel Ziegler, Jeffrey Wu, Clemens Winter, Chris Hesse, Mark Chen, Eric Sigler, Mateusz Litwin, Scott Gray, Benjamin Chess, Jack Clark, Christopher Berner, Sam McCandlish, Alec Radford, Ilya Sutskever, and Dario Amodei. Language models are few-shot learners. In H. Larochelle, M. Ranzato, R. Hadsell, M.F. Balcan, and H. Lin, editors, *Advances in Neural Information Processing Systems*, volume 33, pages 1877–1901. Curran Associates, Inc., 2020.
- [7] John-Marc Chandonia, Lindsey Guan, Shiangyi Lin, Changhua Yu, Naomi K Fox, and Steven E Brenner. SCOPE: improvements to the structural classification of proteins – extended database to facilitate variant interpretation and machine learning. *Nucleic Acids Research*, 50(D1):D553–D559, 12 2021.
- [8] Mark Chen, Alec Radford, Rewon Child, Jeff Wu, Heewoo Jun, David Luan, and Ilya Sutskever. Generative pretraining from pixels. In *Proceedings of the 37th International Conference on Machine Learning, ICML’20*. JMLR.org, 2020.
- [9] Uri Cohen, SueYeon Chung, Daniel D Lee, and Haim Sompolinsky. Separability and geometry of object manifolds in deep neural networks. *Nature communications*, 11(1):1–13, 2020.
- [10] The UniProt Consortium. UniProt: the universal protein knowledgebase in 2021. *Nucleic Acids Research*, 49(D1):D480–D489, 11 2020.
- [11] Jia Deng, Wei Dong, Richard Socher, Li-Jia Li, Kai Li, and Li Fei-Fei. Imagenet: A large-scale hierarchical image database. In *2009 IEEE conference on computer vision and pattern recognition*, pages 248–255. Ieee, 2009.
- [12] N.S. Detlefsen, S. Hauberg, and W. Boomsma. Learning meaningful representations of protein sequences. *Nature Communications*, 13, 2022.
- [13] Jacob Devlin, Ming-Wei Chang, Kenton Lee, and Kristina N. Toutanova. Bert: Pre-training of deep bidirectional transformers for language understanding. *Proceedings of the 2019 Conference of the North American Chapter of the Association for Computational Linguistics: Human Language Technologies*, 1:4171–4186, 2019.
- [14] Diego Doimo, Aldo Glielmo, Alessio Ansuini, and Alessandro Laio. Hierarchical nucleation in deep neural networks. *Advances in Neural Information Processing Systems*, 33, 2020.
- [15] Ahmed Elnaggar, Michael Heinzinger, Christian Dallago, Ghaliya Rehawi, Wang Yu, Llion Jones, Tom Gibbs, Tamas Feher, Christoph Angerer, Martin Steinegger, Debsindhu Bhowmik, and Burkhard Rost. ProtTrans: Towards Cracking the Language of Lifes Code Through Self-Supervised Deep Learning and High Performance Computing. *IEEE Transactions on Pattern Analysis and Machine Intelligence*, 2021.

- [16] Elena Facco, Maria d’Errico, Alex Rodriguez, and Alessandro Laio. Estimating the intrinsic dimension of datasets by a minimal neighborhood information. *Scientific Reports*, 7, 2017.
- [17] Aldo Glielmo, Iuri Macocco, Diego Doimo, Matteo Carli, Claudio Zeni, Romina Wild, Maria d’Errico, Alex Rodriguez, and Alessandro Laio. Dadapy: Distance-based analysis of data-manifolds in python. *Patterns*, 3(10):100589, 2022.
- [18] John Hewitt and Christopher D. Manning. A structural probe for finding syntax in word representations. In *Proceedings of the 2019 Conference of the North American Chapter of the Association for Computational Linguistics: Human Language Technologies, Volume 1 (Long and Short Papers)*, pages 4129–4138, Minneapolis, Minnesota, June 2019. Association for Computational Linguistics.
- [19] Christian Horvat and Jean-Pascal Pfister. Intrinsic dimensionality estimation using normalizing flows. In *Advances in Neural Information Processing Systems*, 2022.
- [20] Yanrong Ji, Zhihan Zhou, Han Liu, and Ramana V Davuluri. DNABERT: pre-trained Bidirectional Encoder Representations from Transformers model for DNA-language in genome. *Bioinformatics*, 37(15):2112–2120, 02 2021.
- [21] Jeff Johnson, Matthijs Douze, and Hervé Jégou. Billion-scale similarity search with GPUs. *IEEE Transactions on Big Data*, 7(3):535–547, 2019.
- [22] John Jumper, Richard Evans, Alexander Pritzel, Tim Green, Michael Figurnov, Olaf Ronneberger, Kathryn Tunyasuvunakool, Russ Bates, Augustin Žídek, Anna Potapenko, et al. Highly accurate protein structure prediction with AlphaFold. *Nature*, 596(7873):583–589, 2021.
- [23] Alexander Kolesnikov, Alexey Dosovitskiy, Dirk Weissenborn, Georg Heigold, Jakob Uszkoreit, Lucas Beyer, Matthias Minderer, Mostafa Dehghani, Neil Houlsby, Sylvain Gelly, Thomas Unterthiner, and Xiaohua Zhai. An image is worth 16x16 words: Transformers for image recognition at scale. *Proceedings of the International Conference on Learning Representations*, 18–24 Jul 2021.
- [24] Zeming Lin, Halil Akin, Roshan Rao, Brian Hie, Zhongkai Zhu, Wenting Lu, Allan dos Santos Costa, Maryam Fazel-Zarandi, Tom Sercu, Sal Candido, et al. Language models of protein sequences at the scale of evolution enable accurate structure prediction. *bioRxiv*, 2022.
- [25] Nelson F. Liu, Matt Gardner, Yonatan Belinkov, Matthew E. Peters, and Noah A. Smith. Linguistic knowledge and transferability of contextual representations. In *Proceedings of the 2019 Conference of the North American Chapter of the Association for Computational Linguistics: Human Language Technologies, Volume 1 (Long and Short Papers)*, pages 1073–1094, Minneapolis, Minnesota, June 2019. Association for Computational Linguistics.
- [26] Jonathan Mamou, Hang Le, Miguel Del Rio, Cory Stephenson, Hanlin Tang, Yoon Kim, and Sueyeon Chung. Emergence of separable manifolds in deep language representations. In *International Conference on Machine Learning*, pages 6713–6723. PMLR, 2020.
- [27] Christopher D. Manning, Kevin Clark, John Hewitt, Urvashi Khandelwal, and Omer Levy. Emergent linguistic structure in artificial neural networks trained by self-supervision. *Proceedings of the National Academy of Science*, 117(48):30046–30054, December 2020.
- [28] Joshua Meier, Roshan Rao, Robert Verkuil, Jason Liu, Tom Sercu, and Alex Rives. Language models enable zero-shot prediction of the effects of mutations on protein function. *Advances in Neural Information Processing Systems*, 34, 2021.
- [29] Alec Radford, Jong Wook Kim, Chris Hallacy, Aditya Ramesh, Gabriel Goh, Sandhini Agarwal, Girish Sastry, Amanda Askell, Pamela Mishkin, Jack Clark, Gretchen Krueger, and Ilya Sutskever. Learning transferable visual models from natural language supervision. In Marina Meila and Tong Zhang, editors, *Proceedings of the 38th International Conference on Machine Learning*, volume 139 of *Proceedings of Machine Learning Research*, pages 8748–8763. PMLR, 18–24 Jul 2021.
- [30] Colin Raffel, Noam Shazeer, Adam Roberts, Katherine Lee, Sharan Narang, Michael Matena, Yanqi Zhou, Wei Li, and Peter J. Liu. Exploring the limits of transfer learning with a unified text-to-text transformer. *J. Mach. Learn. Res.*, 21(1), jun 2022.
- [31] Roshan M Rao, Jason Liu, Robert Verkuil, Joshua Meier, John Canny, Pieter Abbeel, Tom Sercu, and Alexander Rives. MSA Transformer. *Proceedings of the 38th International Conference on Machine Learning*, 139:8844–8856, 18–24 Jul 2021.

- [32] Alexander Rives, Joshua Meier, Tom Sercu, Siddharth Goyal, Zeming Lin, Jason Liu, Demi Guo, Myle Ott, C. Lawrence Zitnick, Jerry Ma, and Rob Fergus. Biological structure and function emerge from scaling unsupervised learning to 250 million protein sequences. *Proceedings of the National Academy of Sciences*, 118(15):e2016239118, 2021.
- [33] Anna Rogers, Olga Kovaleva, and Anna Rumshisky. A primer in bertology: What we know about how bert works. *Transactions of the Association for Computational Linguistics*, 8:842–866, 2020.
- [34] B. Scholkopf and A.J. Smola. *Learning with Kernels: Support Vector Machines, Regularization, Optimization, and Beyond*. Adaptive Computation and Machine Learning series. MIT Press, 2018.
- [35] Konstantin Schütze, Michael Heinzinger, Martin Steinegger, and Burkhard Rost. Nearest neighbor search on embeddings rapidly identifies distant protein relations. *Frontiers in Bioinformatics*, 2, 2022.
- [36] Johannes Söding and Michael Remmert. Protein sequence comparison and fold recognition: progress and good-practice benchmarking. *Current opinion in structural biology*, 21 3:404–411, 2011.
- [37] Ian Tenney, Dipanjan Das, and Ellie Pavlick. BERT rediscovers the classical NLP pipeline. In *Proceedings of the 57th Annual Meeting of the Association for Computational Linguistics*, pages 4593–4601, Florence, Italy, July 2019. Association for Computational Linguistics.
- [38] Ashish Vaswani, Noam Shazeer, Niki Parmar, Jakob Uszkoreit, Llion Jones, Aidan N Gomez, Lukasz Kaiser, and Illia Polosukhin. Attention is all you need. *Advances in Neural Information Processing Systems*, 30, 2017.

A Appendix

Table 1: Characteristics of the models employed for extracting representations.

Model	#Blocks	Emb. dim.	#Heads	#Params	Dataset	Reference
ProtBert	30	1024	16	420M	UR100	[15]
ProtT5-XL-U50	24	1024	32	3B	UR50 BFD	[15]
ESM-1b	33	1280	20	650M	UR50/D	[32]
ESM-1v	33	1280	20	650M	UR90	[28]
ESM-2(8M)	6	320	20	8M	UR50/D	[24]
ESM-2(35M)	12	480	20	35M	UR50/D	[24]
ESM-2(150M)	30	640	20	150M	UR50/D	[24]
ESM-2(650M)	33	1280	20	650M	UR50/D	[24]
ESM-2(3B)	36	2560	40	3B	UR50/D	[24]
ESM-2(15B)	48	5120	40	15B	UR50/D	[24]
iGPT-S(76M)	24	512	8	76B	ImageNet	[8]
iGPT-M(455M)	36	1024	8	455B	ImageNet	[8]
iGPT-L(1.4B)	48	1536	16	1.4B	ImageNet	[8]

A.1 Experimental setup

Hardware All experiments were performed on a machine with 2 Intel(R) Xeon(R) Gold 6226 with a total of 48 threads, 256GB RAM equipped with 2 Nvidia V100 GPUs with 32GB memory, hosted on the ORFEO supercomputing platform at AREA Science Park. The GPUs were used to generate embeddings and to compute nearest neighbors.

A.2 Experiments

Two Nearest Neighbors ID estimator To estimate the intrinsic dimension of hidden representations, we use the Two-Nearest Neighbors-Based (TwoNN) ID estimator [16]. The algorithm is based on a simple analytical result: under the hypothesis of a uniform density of points in \mathbb{R}^d , the cumulative probability distribution of the random variable $\mu = \frac{r_2}{r_1}$, where r_1, r_2 are respectively the distance to the first and the second neighbor of a given point, is given by $F(\mu) = 1 - \mu^{-d}$. Therefore, for a given dataset whose points are indexed by $i = 1, \dots, N$ in \mathbb{R}^D (with $D \gg d$ in interesting cases), we compute for each point the ratios μ_i , sort them in ascending order with a permutation σ , and, by defining the empirical cumulative distribution $F^{emp}(\mu_{\sigma(i)}) := \frac{i}{N}$, we can obtain an estimate of d as the slope given by a linear regression (passing through the origin) of the following variables: $(\log(\mu_i), -\log(1 - F^{emp}(\mu_i))) | i = 1, \dots, N$. The TwoNN algorithm requires minimal information: the distances to each point’s first and second nearest neighbor; therefore, the strong hypothesis of a uniform density used to obtain the main result can be relaxed to a weak assumption of *local* uniformity. We estimate the ID and its reliability through a progressive, random decimation process that allows testing the stability of the result with respect to a change in spatial scale. Since the estimate is approximately scale-invariant, we take the ID estimate as the mean over the values collected during the decimation.

GPU kNN search The nearest neighbor searches for the calculation of the neighborhood overlap as in [17] were carried out by means of the Python interface of the Facebook AI Similarity Search library [21], version 1.7.2. The library is particularly suited for large datasets embedded in high dimensions since it is based on a reliable approximate and extremely fast similarity search procedure.

A.3 Further results

A.3.1 The ID shape for different pLMs architectures

The latest developments in the application of pre-trained pLMs for the solution of diverse biological tasks have been fuelled by two families of models: Prot-Trans [15] and Evolutionary Scale Modelling (ESM) [32, 31, 28, 24]. During the last years pLMs with different architectures, number of parameters,

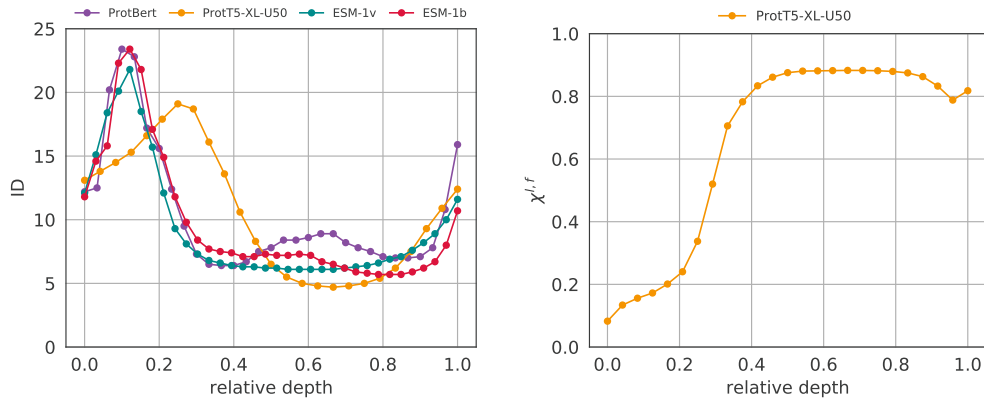


Figure 5: Further experiments. [Left] The ID curves for different pLMs trained on different datasets consistently show the three-phased behavior consisting of a peak, a plateau, and a final ascent. [Right] First nearest neighbor SCOPE super-family retrieval accuracy of Prot-T5-XL-U50 is higher in plateau layers.

and embedding sizes have been trained on several datasets obtained starting from the UniProt [10] database. In Fig. 5 we complement our analysis in section 3.1.1 including several models whose architectural details and training strategies are described in Table 1. Despite the significant differences of the pLMs considered in the analysis, the consistency of the three-phased behavior of the ID curve is remarkable: an initial peak is followed by a plateau where the ID assumes low values, and the ID grows again to values close to the one measured after the positional embedding.

A.3.2 Nearest neighbor search in plateau layers improves identification of protein relations

It was recently shown in [35] that first nearest neighbor searches for remote homologous protein domains based on the last hidden layer representations of the ProtT5-XL-U50 pLM outperform state-of-the-art methods based on sequence similarity. Adapting the approach in 3.2.1, we mimic the experiment performed in Section 2 of [35] by 1) considering protein domains in SCOPE belonging to a super-family with at least 2 sequences, 2) setting the number of neighbors to $k = 1$. Considering representations in the plateau layer improves the accuracy of the 1-kNN homology search. In particular, in Fig. 5 [Right] we observe an improvement of $\approx 6\%$ performing the search on a plateau layer instead of the last layer before the output.